The Stiffness of Rabbit Skeletal Actomyosin Cross-Bridges Determined with an Optical Tweezers Transducer

Claudia Veigel, Marc L. Bartoo, David C. S. White, John C. Sparrow, and Justin E. Molloy
Department of Biology, University of York, York YO1 5YW, England

ABSTRACT Muscle contraction is brought about by the cyclical interaction of myosin with actin coupled to the breakdown of ATP. The current view of the mechanism is that the bound actomyosin complex (or "cross-bridge") produces force and movement by a change in conformation. This process is known as the "working stroke." We have measured the stiffness and working stroke of a single cross-bridge (κ_{xb}, d_{xb}, respectively) with an optical tweezers transducer. Measurements were made with the "three bead" geometry devised by Finer et al. (1994), in which two beads, supported in optical traps, are used to hold an actin filament in the vicinity of a myosin molecule, which is immobilized on the surface of a third bead. The movements and forces produced by actomyosin interactions were measured by detecting the position of both trapped beads. We measured, and corrected for, series compliance in the system, which otherwise introduces large errors. First, we used video image analysis to measure the long-range, force-extension property of the actin-to-bead connection (κ_{con}), which is the main source of "end compliance." We found that force-extension diagrams were nonlinear and rather variable between preparations, i.e., end compliance depended not only upon the starting tension, but also upon the F-actin-bead pair used. Second, we measured κ_{xb} and κ_{con} during a single cross-bridge attachment by driving one optical tweezer with a sinusoidal oscillation while measuring the position of both beads. In this way, the bead held in the driven optical tweezer applied force to the cross-bridge, and the motion of the other bead measured cross-bridge movement. Under our experimental conditions (at ~2 pN of pretension), connection stiffness (κ_{con}) was 0.26 ± 0.16 pN nm^{-1}. We found that rabbit heavy meromyosin produced a working stroke of 5.5 nm, and cross-bridge stiffness (κ_{xb}) was 0.69 ± 0.47 pN nm^{-1}.

INTRODUCTION

Many types of cellular motility, including muscle contraction, are driven by the cyclical interaction of myosin with actin, coupled to the breakdown of ATP. The current view of the mechanism is that myosin binds to actin with the products of ATP hydrolysis (ADP and phosphate) bound in the catalytic site (cross-bridge attachment). Then, as the products are released, myosin changes conformation to produce a movement or "working stroke" (Huxley, 1969). In the absence of nucleotide, actin and myosin form a tightly bound "rigor" complex. Binding of a new ATP molecule to myosin causes the rigor complex to dissociate (cross-bridge detachment), and subsequent ATP hydrolysis resets the original myosin conformation so that the cycle can be repeated (Lymn and Taylor, 1971). During the cycle, part of the cross-bridge becomes distorted by the working stroke, and mechanical work is stored in this elastic deformation. In this way, the cross-bridge captures the sudden changes in chemical potential associated with steps in the biochemical cycle and is able to do external work on a much slower time scale, e.g., as muscle shortens or vesicles are transported (Huxley and Simmons, 1971). There are three key features to this mechanism; 1) one ATP molecule is broken down per mechanical cycle; 2) the size of the working stroke is determined by the conformation of myosin at the start and end of the attached period; 3) the cross-bridge is elastic (see review by Cooke, 1998).

Important issues in our understanding of the cross-bridge mechanism are the size of its working stroke and the force that it can produce. Recently, several laboratories have developed single-molecule mechanical transducers that are based on either "optical tweezers" (laser traps) or glass microneedles (e.g., Finer et al. 1994; Saito et al. 1994; Molloy et al., 1995; Ishijima et al., 1996; Dupuis et al., 1997). An advantage of single-molecule experiments over muscle fiber experiments is that the force, working stroke, and kinetics of a single cross-bridge interaction can be measured directly. Measurements of such individual interactions allow critical tests to be made of how actomyosin converts chemical energy to mechanical work. For example, the myosin working stroke should be smaller than the span of a single cross-bridge (a myosin head or S1 is ~16 nm long; Rayment et al., 1993), and the mechanical work done by each cross-bridge interaction must be less than that produced by the breakdown of one ATP molecule. This requires that the elastic element (κ_{xb}) should be of the correct stiffness to store a suitable fraction of the free energy available from ATP breakdown measured under physiological chemical conditions.

The mechanical arrangement used to study actomyosin interactions in most optical tweezer transducers is based on the "three bead" geometry devised by Finer et al. (1994) (see Fig. 1). A single actin filament is suspended between two beads, each held in an independent optical trap (we define these, arbitrarily, as "left" and "right" traps). The filament is positioned above a third bead, on which myosin

Received for publication 30 July 1997 and in final form 19 June 1998.
Address reprint requests to Dr. Justin E. Molloy, Department of Biology, University of York, P.O. Box 373, York YO1 5YW, England.
© 1998 by the Biophysical Society
0006-3495/98/09/1424/15 $2.00

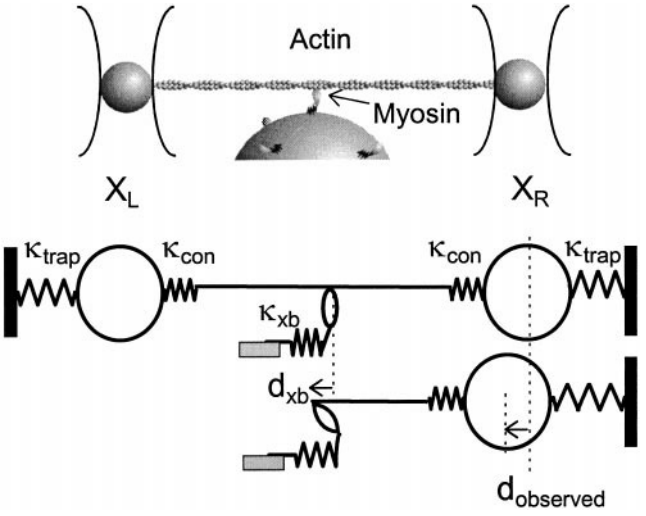

FIGURE 1 The upper panel is a cartoon showing the "three-bead geometry" devised by Finer et al. (1994), used to make single-molecule mechanical measurements from actomyosin. Two latex beads holding an actin filament are manipulated in two independent optical traps. This makes it possible to bring the filament into the vicinity of a third, larger bead that is fixed to the surface of the experimental chamber. The "third bead" is coated with myosin molecules at a low surface density. Actomyosin interactions are monitored by observing the position of the trapped beads with a photodetector (giving the bead positions, X_L and X_R). The lower panel represents the mechanical elements of the system. Upon binding to actin, the myosin cross-bridge forms a mechanical pathway between the beads that are suspended in the optical traps and "ground." The cross-bridge stiffness, κ_{xb}, is linked in series with the actin-to-bead connection stiffness, κ_{con}, and these are combined in parallel with the optical trap stiffness, κ_{trap}. This combination of "springs" gives the overall mounting stiffness κ_x. A fraction of the cross-bridge working stroke, d_{xb}, is taken up by the compliance of the connection, and therefore observed bead displacements ($d_{observed}$) measured with the photodetector need to be corrected for the effects of series compliance in the system.

is deposited at low surface density. This geometry is required to study skeletal muscle myosin (and other motors that spend only a small proportion of their time attached), as it prevents actin from diffusing away from myosin during the detached period of the cross-bridge cycle. Movement and force produced by single cross-bridge interactions are inferred from the position of at least one bead, which is monitored by imaging it onto a quadrant photodiode (4QD). The detector determines the position of the centroid of the image to a resolution of better than 0.5 nm.

Published estimates of the working stroke vary between 5 nm and 25 nm, estimates of stiffness range from 0.16 to 0.6 pN nm^{-1}, and maximum force ranges from 1 to 5 pN (Finer et al., 1994; Guilford et al., 1997; Mehta et al., 1997; Molloy et al., 1995; Nishizaka et al., 1995; Saito et al., 1994; Simmons et al., 1996). Variability in these data between laboratories may, in part, be explained by differences in the type of myosin or subfragment used. However, there are also systematic complications in the measurements, and these have been dealt with in different ways.

1. To determine the cross-bridge working stroke, the stiffness of the apparatus (here the optical traps) must be much less than that of the cross-bridge (e.g., $\kappa_{trap} \ll \kappa_{xb}$; Fig. 1). This makes it possible for the cross-bridge to undergo its full working stroke unhindered. At such low trap stiffness the beads and associated actin filament necessarily exhibit large amounts of Brownian motion. Determinations of the working stroke depend upon how Brownian motion is accounted for in the analysis (Molloy et al., 1995; Ishijima et al., 1996; Guilford et al., 1997; Mehta et al., 1997).

2. Determinations of the maximum force developed by a cross-bridge under isometric conditions (i.e., no net movement of the molecule) require that the apparatus stiffness is much greater than that of the cross-bridge. This means that the cross-bridge is prevented from moving, allowing its maximum force to be developed. Although the stiffness of the trap can be made sufficiently high by applying feedback ($\kappa_{trap} \approx 10$ pN nm^{-1}; Simmons et al., 1996), the stiffness of the attachments of actin to the two beads is likely to be much smaller (Dupuis et al., 1997; Veigel et al., 1997). Low "connection stiffness" (κ_{con}; Fig. 1) allows movement of the cross-bridge and thus reduces the size of the observed movement and force that it can produce.

To obtain a good estimate of cross-bridge stiffness, κ_{xb}, we have measured and corrected for sources of series elasticity in the system. We have lumped the series elasticity into one component, termed κ_{link}. This consists of the series combination of the actin filament stiffness, κ_{actin}, and the stiffness of its connection to the trapped bead, κ_{con}. We have also refined our measurement of cross-bridge working stroke, d_{xb}, by using position information obtained from both beads. To make these measurements we have developed our apparatus to monitor the positions of both trapped beads simultaneously. One method uses analysis of video images to obtain a linear position signal over a long range (up to 12 μm); and another uses two four-quadrant photodetectors to make high-speed measurements of each trapped bead over a fairly short distance (up to 1 μm). These developments have enabled us to:

1. Determine the compliance of the connection between the NEM-modified myosin-coated beads and the actin filament used in our experiments, e.g., κ_{con}.

2. Determine cross-bridge stiffness (κ_{xb}) by measuring its movement when subjected to an applied load during a single binding event.

3. Test if the length of actin remains constant during its interaction with myosin under low-load conditions.

We discuss the implications of our single-molecule mechanical study in the context of current ideas of the mechanism of force production by actomyosin, which derive mainly from work with muscle fibers.

MATERIALS AND METHODS

Optical tweezers transducer

Our optical tweezers transducer is based around an inverted, fluorescence microscope (Fig. 2). A key feature is that most of the apparatus is computer controlled. This allows different kinds of experiments to be performed simply by running different software.

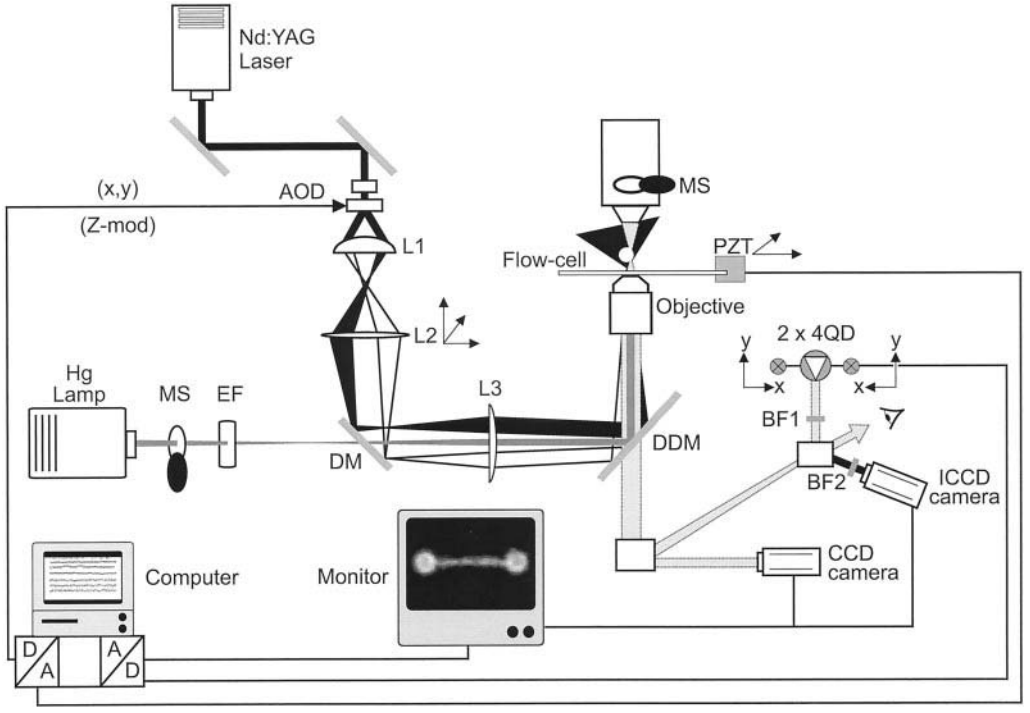

FIGURE 2 The optical trap is built around an inverted microscope (Axiovert 135; Zeiss, Germany). Infrared (1064 nm) laser light, from a diode-pumped Nd:YAG laser (Adlas Model 321, 1064 nm; Adlas, Lubeck, Germany) is combined with green light (EF = 546FS10.25, excitation filter; Andover Corp., Salem, NH) from a mercury arc lamp by use of a "hot mirror" (DM = 820DCSP; Omega Optical, Brattleboro, VT). Both light beams enter the microscope epifluorescence port via a custom-built housing. A dual dichroic mirror (DDM = 570DCLP, Omega; reflects 546 nm and 1064 nm; transmits >570 nm), mounted in the microscope filter block, allows us to use optical tweezers and view rhodamine fluorescence simultaneously. Laser beam alignment is via two mirrors, and the trap position is controlled with two orthogonally mounted acoustooptic deflectors (AODs) (synthesiser/driver, N64010–100 2ASDFS-2, TeO_2 crystals N45035-3-6.5 DEG-1.06; NEOS Technologies) controlled by a custom-built computer interface card. To produce two optical traps, we chop between two sets of *x*, *y* coordinates (to simplify computation, these coordinates are chopped in hardware at 10 kHz). The laser light path is completely enclosed with cardboard tubing to prevent air currents from entering the system at any point. Coarse control of the stage position is by mechanical drives, and a custom-built piezoelectric substage (PZT) allows small range computer-controlled movements of the microscope slide. High-speed position measurements are made with four-quadrant photodiode detectors (2 × 4QD = S1557, Hamamatsu Photonics, Hamamatsu City, Japan; and custom-built electronics). The image is split in half with a 90°, front-surface mirrored, Amici prism, and images of the left and right beads are projected onto the two detectors. Scattered laser light is excluded with a barrier filter (BF1 = short-pass barrier filter). Actin fluorescence was visualized with an intensified CCD camera (Photon-P46036A; EEV, Chelmsford, UK) coupled to a barrier filter (BF2 = LP590; Zeiss). Bright-field illumination (100-W halogen lamp) is used to produce a high-magnification video image (CCD camera, P46310; EEV). An Acroplan 100×, 1.3 N.A. objective and an Optovar 2.5× insert are used to obtain the desired image magnification. Video images from the half-inch format CCD camera attached to the camera port are captured at 512 × 512 pixel resolution, giving 1 pixel = 26 nm. A "slotted-opto switch" detects the position of the microscope prisms used to select different TV/camera ports and permits computer control of mechanical shutters (MS) used to switch between bright-field and fluorescence illumination and of the video source. The 4QDs, AODs, PZT, etc. were cross-calibrated with the video "frame-grabber."

In overview, a single actin filament was attached at either end to two 1.1-μm latex beads that were held and manipulated by two independently controlled optical tweezers. The filament was positioned over a third (glass) bead that was fixed to the surface of the experimental chamber. This bead had been sparsely coated with rabbit heavy meromyosin (HMM) molecules (see Fig. 1). Mechanical interactions between a single HMM molecule and the actin filament were detected from the motion of a bright-field image of the two latex beads cast onto two four-quadrant photodiode detectors (4QD).

Optical tweezers and beam steering

Two independent optical tweezers were synthesized by chopping a single laser beam between two sets of *x, y* coordinates (see Molloy, 1997, for details) with acoustooptical devices (NEOS Technologies, Melbourne, FL). These were controlled by a custom computer interface card with two sets of digital output registers (loaded with the two *x, y* coordinates) that were multiplexed at 10 kHz.

In this paper, stiffness measurements were made by applying a large-amplitude sinusoidal forcing function to one optical tweezer. For this method to work there were three requirements: 1) fast and stable control of the trap position; 2) linearity of the detector signal over the range ± 200 nm; 3) good stage stability over the time course of the experiment. We deal with these issues below.

Acoustooptical deflectors

Acoustooptical deflector (AOD) control of laser position is extremely rapid (response time ≈ 2 μs). However, we found that drift and noise in laser position arose from a variety of sources, including laser pointing stability, AOD noise, and mechanical drift (between the axis of the microscope and the rest of the optical path). We measured the sum of all of these sources of noise (Fig. 3 *A*) and found that stability depended critically upon excluding air currents from the light path; drift was <0.5 nm s^{-1}; noise was <1 nm rms (Fig. 3 *A*).

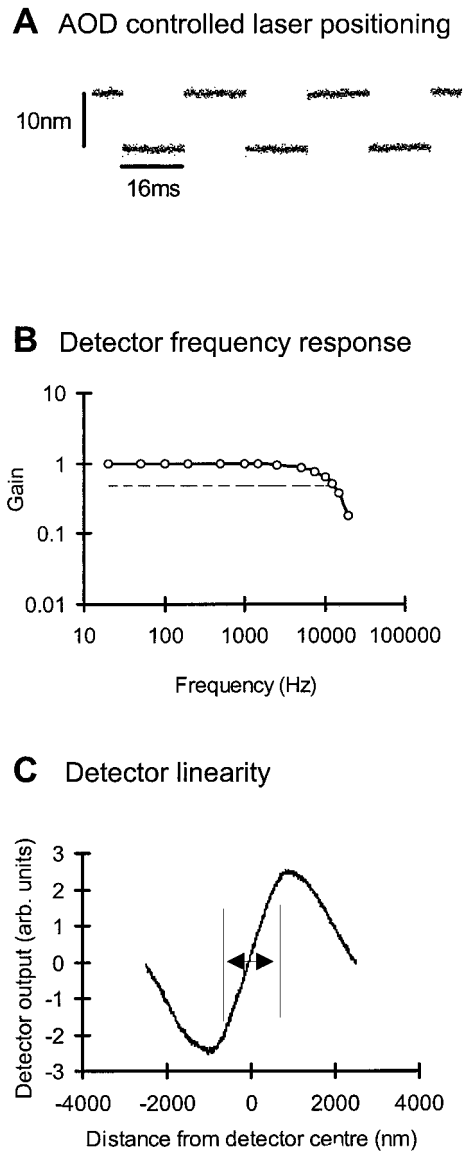

FIGURE 3 (*A*) The speed and stability of AOD-controlled laser positioning were tested by moving the laser beam in a square wave function (30 Hz). The laser beam was reflected from the surface of a silvered coverslip at the microscope object plane and projected onto one of the two 4QDs. The illumination intensity was made the same as that obtained from the bead image. This measures tweezer stability relative to the microscope axis (data sampled at 50 kHz). (*B*) The detector bandwidth was determined over the range of 10 Hz to 20 kHz with the reflected laser beam (as in *A*). The beam position was varied sinusoidally using the AODs, and the input/output response was determined from the discrete Fourier transform of the data (data sampled at 50 kHz). (*C*) The linearity of the detectors was determined by capturing a latex bead and then moving the bead back and forth with a large-amplitude triangular wave form (± 3 μm). Twenty cycles were averaged to obtain the graph; residual noise is attributable to Brownian motion of the trapped bead.

Four-quadrant photodetectors

We used two four-quadrant photodetectors (4QD) so that the positions of both beads holding the actin filament could be measured. Beads were positioned such that their images lay on either side of the midline of the field of view. The microscope image was split using a mirrored Amici prism (Fig. 2), and each half-image was projected onto a detector. The detectors could be translated along the x (or y) axis to accommodate different lengths of actin filament. Changes in the illumination of the four quadrants were used to measure the bead translation parallel (x) and perpendicular (y) to the actin filament (using electronics similar to those of Simmons et al., 1996). The gain and frequency response of both detectors were matched by adjusting their signal for the same trapped bead.

The response of the 4QDs was found to be linear over a range of ± 300 nm from the detector center (see Fig. 3 *C* for details). This exceeded the maximum range used in our experiments. Detector gain was flat to 10 kHz ($f_c \approx 12.5$ kHz; Fig. 3 *B*), i.e., much greater than the bandwidth of Brownian motion (≈ 600 Hz). Detector noise has both electrical ("dark" noise) and optical (shot noise) sources. We measured the sum of these by evenly illuminating the 4QD (at about the same intensity of light obtained when the bead image is cast on the detector) and recording the output signal (Fig. 4 *A*). The power density spectrum of this noise is shown in Fig. 4 *D*. The bandwidth of the noise is governed by the electronics of the detector circuit. We chose feedback resistors of 100 MΩ ($= R$) in our current-to-voltage "head-stage" circuit. This gave the best compromise between bandwidth (proportional to $1/R$), gain (proportional to R), and resistor noise (Johnson noise, proportional to $R^{0.5}$). Detector noise was $\sim$100-fold smaller than the Brownian motion of the bead, and so minimal correction for detector response was required.

Microscope substage

The final positioning of the HMM-coated bead beneath the suspended actin filament was made using a computer-controlled piezoelectric substage. The range of movement was 25×25 μm^2. Control was by two 12-bit D/A converters (Data Translation; DT2812A) producing 6 nm of displacement per digital bit. Stage position noise (>1 Hz and <10 kHz) was 0.9 nm root mean square (r.m.s.), but long-term stability was poor (~ 0.5 nm $\cdot$ s^{-1}; data not shown). This meant that measurements of individual cross-bridge events lasting between 1 ms and 1 s were essentially free of stage positional noise. However, during the course of a single experiment lasting up to 2 h, the stage had to be repositioned several times.

Preparation of proteins, coated beads, experimental chambers, and solutions

F-actin, whole myosin, and HMM were prepared from rabbit skeletal muscle by standard methods (Pardee and Spudich, 1982; Margossian and Lowey, 1982).

Preparation of NEM-myosin

Rabbit skeletal muscle myosin was precipitated from 50 μl of stock solution (25 mg ml^{-1} myosin, stored at -20°C in buffered salt solution containing 50% glycerol, prepared as described by Margossian and Lowey, 1982) by the addition of 500 μl of deionized water. The pellet was resuspended in "high salt" buffer (HiS) (500 mM KCl, 4 mM $MgCl_2$, 1 mM EGTA, 20 mM K phosphate buffer, pH 7.2) to give a final concentration of 12 mg ml^{-1}. To this, *N*-ethyl-maleimide (from freshly made 100 mM stock; Sigma Chemical Co.) was added to a final concentration of 4 mM (Meeusen and Cande, 1979). The solution was incubated at 20°C for 30 min, and the reaction was stopped by the addition of 500 μl of 20 mM dithiothreitol in deionized water. The NEM-modified myosin pellet was resuspended in HiS to give a final protein concentration of 80 μg ml^{-1}.

Preparation of NEM-myosin-coated "C-beads"

To make the 1.1-μm polystyrene beads (plain latex beads; LB11 Sigma Chemical Co.) bind to F-actin irreversibly, they were coated with NEM-modified myosin. Ten microliters of beads (10% by mass) was washed twice in 100 μl of deionized water and collected by spinning at $8000 \times g$

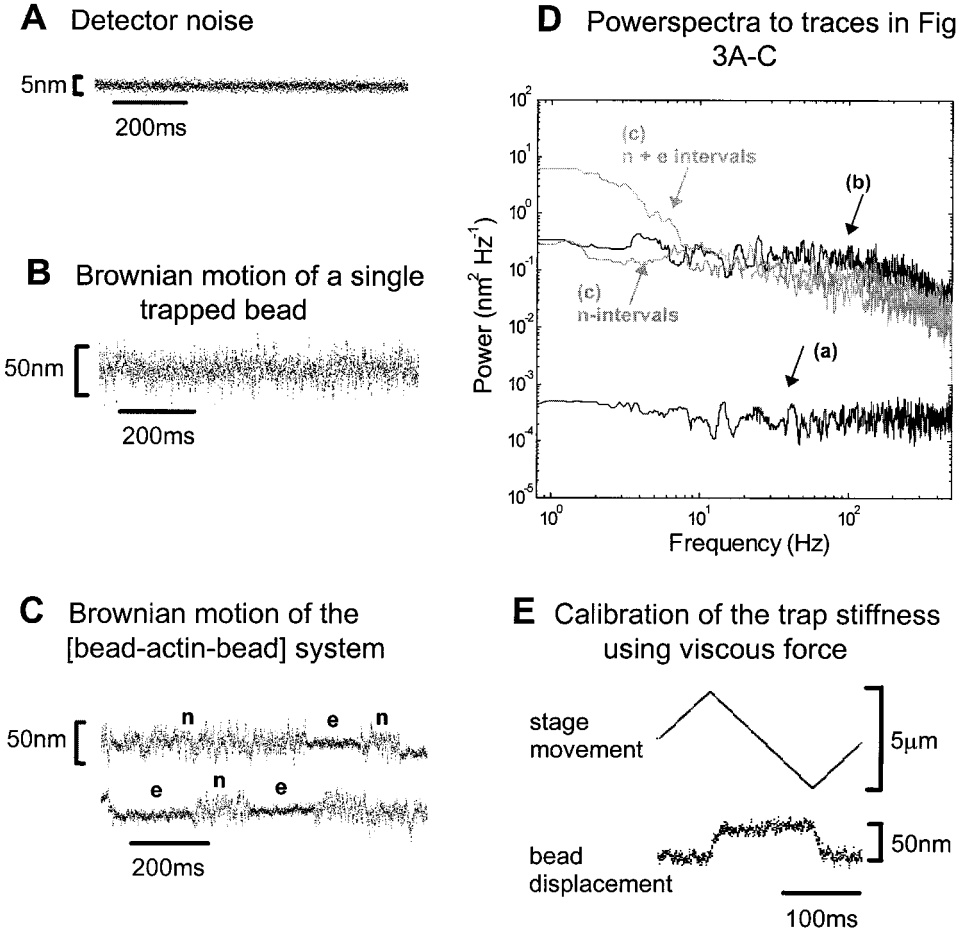

FIGURE 4 Analysis of noise sources in the system in the time and frequency domain. (*A*) Detector noise at full illumination: 1.4 nm rms. (*B*) Brownian noise of a single trapped bead. The r.m.s. deviation in position measured on one axis, over a period of 2.4 s at 2.5 kHz bandwidth, was 14 nm, giving a trap stiffness of 0.02 pN nm^{-1} (5 kHz sample rate). (*C*) Brownian noise of the bead-actin-bead system. *n* indicates intervals of high noise (in the absence of cross-bridge attachment, 11 nm rms. *e* indicates intervals of reduced noise (in the presence of an attached cross-bridge, 3 nm r.m.s. (measured at 3 μM ATP)). (*D*) Spectral analysis of traces in *A–C*. *Trace a*: Detector noise, corner frequency $f_c \approx 12.5$ kHz. *Trace b*: Spectrum for a trapped bead, heavily damped with $f_c \approx 300$ Hz; trap stiffness = 0.02 pN nm^{-1}. *Trace c*: Spectrum of Fig. 3 *C* (*n* + *e* periods); note that there are two corner frequencies, $f_{c1} \approx 3$ Hz and $f_{c2} \approx 200$ Hz. (*E*) Calibration of trap stiffness using viscous force. *Upper trace*: 5 Hz triangular waveform motion applied to the piezo substage (4.8 μm peak to peak). *Lower trace*: Bead displacement in the *x* direction (average of 10 cycles). The bead moved ~50 nm peak to peak, giving a trap stiffness of 0.02 pN nm^{-1}.

for 1–2 min. This procedure removed most of the surfactant present in the proprietary buffer. The washed beads were resuspended in 50 μl of deionized water (now ~2% by mass). Ten microliters of washed beads was added to 10 μl of NEM-myosin solution (above), and to this 2.5 μl of 0.1 mg ml^{-1} bovine serum albumin–tetramethylrhodamine isothiocyanate (BSA-TRITC) (Sigma) was added. The solution was finally made up to 100 μl with HiS (final solution contains 0.2% beads (2.7×10^6 beads μl^{-1}), 8 μg ml^{-1} NEM-myosin, 2.5 μg ml^{-1} BSA-TRITC) and incubated overnight at 4°C. The resulting C-beads were washed twice and resuspended in assay buffer (AB) (25 mM KCl, 4 mM $MgCl_2$, 1 mM EGTA, 25 mM imidazolium-chloride, pH 7.4; Kron et al., 1991). Storage of C-beads in low-salt solution as opposed to HiS gave much better stability (they behaved well in our experiments for ~4 days), and the stiffness of the actin-bead connection was improved. Short NEM-myosin filaments might project from the surface of such beads. However, the beads tended to aggregate and required dispersion by bath ultrasonication (duration 1–2 s) just before use.

Flow cell construction

The microscope flow cell was constructed from a precleaned 22×50 mm^2 glass microscope slide across which two 3×22 mm^2 strips of (no. 1) coverglass were fixed 15 mm apart with 2 μl of UV-curing epoxy adhesive. A 22×40 mm^2 precleaned coverslip was coated on one surface with 2 μl of 0.1% nitrocellulose dissolved in amyl acetate (Kron et al., 1991). This solution also contained a suspension of 1.7 μm glass microspheres (Bangs Labs, Carmel, IN); ~2 mg ml^{-1} gave a surface density of about one microsphere per 10 μm^2. The precoated coverslip was glued to the coverglass strips, orthogonally to the slide, leaving ~10 mm of coverslip projecting from either side. The flow cell was exposed to UV light until the glue was completely cured. UV-curing epoxy adhesive was superior to grease for *z* axis (focus) stability during the experiments.

Solutions

Rabbit skeletal HMM (Margossian and Lowey, 1982) was bound to the nitrocellulose-coated coverglass by allowing 100 μl of 1 μg ml^{-1} HMM dissolved in AB to flow into the flow cell and incubating for 1 min. The coverslip surface was then "blocked" by allowing 100 μl of 1 mg ml^{-1} BSA in AB to flow into the flow cell and leaving for 2 min. Finally, 100 μl of AB-GOC solution was added. AB-GOC solution was prepared as follows. AB was degassed with a vacuum pump, and then an oxygen scavenger system, to reduce photobleaching, of 20 mM DTT, 0.2 mg ml^{-1} glucose oxidase, 0.05 mg ml^{-1} catalase, and 3 mg ml^{-1} glucose was added, together with an ATP backup system (2 mM creatine phosphate, 0.1 mg ml^{-1} creatine phosphokinase). This solution was stored in a disposable 1-ml hypodermic syringe fitted with a narrow-bore needle to reduce oxygen diffusion into the buffer. Before the experiment, 2 μl of rhodamine-phalloidin-labeled actin (Molecular Probes; actin concentration 5 μg ml^{-1}), 2 μl of C-beads (above), and ATP at final concentrations between 1 μM and 10 μM were added to 100 μl of AB-GOC. It was important to proceed fairly quickly after the final solution had been added to the flow cell, because the C-beads tended to stick to the coverslip surface. The laboratory was air-conditioned, and the experimental temperature was kept at 23°C.

Optical tweezers procedure

Using fluorescence microscopy, we captured two NEM-myosin-coated beads in the optical tweezers and suspended an actin filament between them. Most of this procedure was performed with the traps held in fixed positions and by steering the stage with the *x-y* mechanical controls. To capture a bead without having to switch the laser tweezer off and on, the bead image was defocused (so the bead lay in a plane between objective and tweezer) just before capture, so that optical scattering forces then acted to push the bead into the stable trapping position. A pretension of 2 pN was applied to the suspended actin filament by moving one of the traps in the *x* direction (along the actin filament axis) and monitoring the motion of the bead held in the stationary trap. The bead-actin-bead assembly was then moved such that each image was cast near or on its respective 4QD. Final alignment of the photodetectors was made using two *x-y* mechanical translators (Fig. 2).

Next, a suitable surface-bound, HMM-coated "third" bead had to be found and positioned beneath the taut actin filament. Surface beads were visualized by bright-field microscopy. To prevent the bead-actin-bead assembly from touching the coverslip surface, the condenser aperture was "stopped down" with the iris diaphragm to give a good depth of focus. The coverslip surface was then surveyed for surface-bound microspheres, at a defocus of ~5 μm. A suitable "third" bead was positioned under the actin filament with the computer-controlled piezo-substage. The condenser aperture was fully opened to allow accurate *z* axis (focus) control, and the focus was adjusted until actomyosin interactions were observed on the highly magnified, bright-field video image of the beads.

Calibration of trap stiffness (κ_{trap})

κ_{trap} was determined by three methods, using a single bead with no actin filament attached (as described by Svoboda and Block, 1994):

1. Stoke's force ($F = \beta v$; v = velocity; $\beta = 6\pi\eta\alpha \approx 10^{-5}$ pN s nm^{-1}; η = viscosity of the solution, α = bead radius) was generated by applying a large-amplitude triangular waveform to the microscope substage, with the trapped bead held 5 μm from the coverslip surface (Fig. 4 *E*). Large forces and motions are produced by this technique, so effects of instrumental noise and calibration errors are minimized.

2. Mean squared Brownian motion ($\langle x^2 \rangle$) was measured and the equipartition principle applied ($\kappa_{trap}\langle x^2 \rangle/2 = \frac{1}{2}kT$) (Fig. 4 *B* and Eq. A3). Data were recorded over a period of several seconds at a bandwidth greater than 2 kHz. Corrections were made for the instrumental noise, which adds to this signal. Because the trap compliance is proportional to x^2, detector noise and calibration are critical to accuracy and errors are worst at high stiffness.

3. With the trapped bead held 5 μm from the coverslip, the power spectrum of the Brownian noise ($f_c = \kappa_{trap}/2\pi\beta$) was determined (Fig. 4 *D*). This method cannot be used to estimate stiffnesses during experiments because the beads are then at an uncertain distance from the coverslip and therefore the viscosity is unknown.

We found that trap stiffness was directly proportional to laser power (data not shown). Experiments were performed using a trap stiffness, κ_{trap}, of 0.02 pN nm^{-1} by adjusting the laser output power and using methods 1–3 (above) to calibrate the stiffness. This was sufficiently lower than the cross-bridge stiffness, to allow good estimates of the working stroke to be made.

RESULTS

Series elasticity and cross-bridge mechanical properties were determined from three different types of measurement.

1. The long-range force-extension property of the bead-actin-bead assembly was measured by moving one laser trap to apply an increasing force and measuring the resulting extension by video image analysis to determine both bead positions.

2. Cross-bridge stiffness and series elasticity of the bead-actin-bead assembly were measured during individual cross-bridge interactions. We used the two four-quadrant photodetectors to measure both bead positions with high time resolution. We determined the stiffnesses either by analysis of the Brownian motion of the beads or by application of a sinusoidal oscillation to the position of one of the laser traps while simultaneously measuring the positions of both of the trapped beads.

3. We measured the working stroke, using the two four-quadrant detectors to monitor both bead positions. By doing this we addressed some of the uncertainties and possible artifacts surrounding our earlier measurements (e.g., Molloy et al., 1995) made with a single detector.

Long-range force-extension property of the actin-to-bead connection, κ_{con}

We measured the long-range force-extension property of the bead-actin-bead assembly by holding one optical trap fixed and applying force by moving the other trap in stepwise increments of 50 nm. The positions of both beads were measured by capturing bright-field video images of the beads and calculating their centers of mass. The applied force was derived from the displacement of the bead held in the fixed trap (from the trap center) and the extension from the distance between the two bead images (see Fig. 5, *A–C*, for details). The gradient of the force-extension diagrams (e.g., Fig. 5 *D*) gave the lumped stiffness of the bead-actin-bead assembly; $\kappa_{link} = \kappa_{actin}\kappa_{con}/(2\kappa_{con} + \kappa_{actin})$ (see Fig. 11 and Eq. A4). These plots were nonlinear, and connection stiffness was greatest at high tension. It would be advantageous to apply large pretensions to the bead-actin-bead assembly and thereby minimize the series compliance. However, to measure the unhindered cross-bridge working stroke, a low-stiffness optical trap is required, and because optical traps only work over a short range (~250 nm), the maximum stable tension that could be applied was ~2 pN. At this tension (Fig. 5 *D*, *dashed box*) the average value of κ_{link} was 0.13 ± 0.06 pN nm^{-1} (n = 18 different actin filaments).

The shape of the force-extension plots (increase in stiffness with increasing force) was variable between preparations, even though actin filament lengths were similar (4.3 ± 0.4 μm). This implies that variability of the plots was due mainly to differences in the connection stiffness κ_{con} and not to differences in actin filament stiffness κ_{actin}. If we make the simplifying assumption that κ_{con} is the same at both ends and that κ_{actin} is much larger (~8 pN nm^{-1} for a 5-μm filament; Kojima et al., 1994), then the stiffness at each end $\kappa_{con} \approx 2 \times \kappa_{link} = 0.26$ pN nm^{-1}. This is more than 10 times larger than κ_{trap} and is consistent with the observation that the amplitude of Brownian motion of the bead-actin-bead assembly corresponds to the sum of both

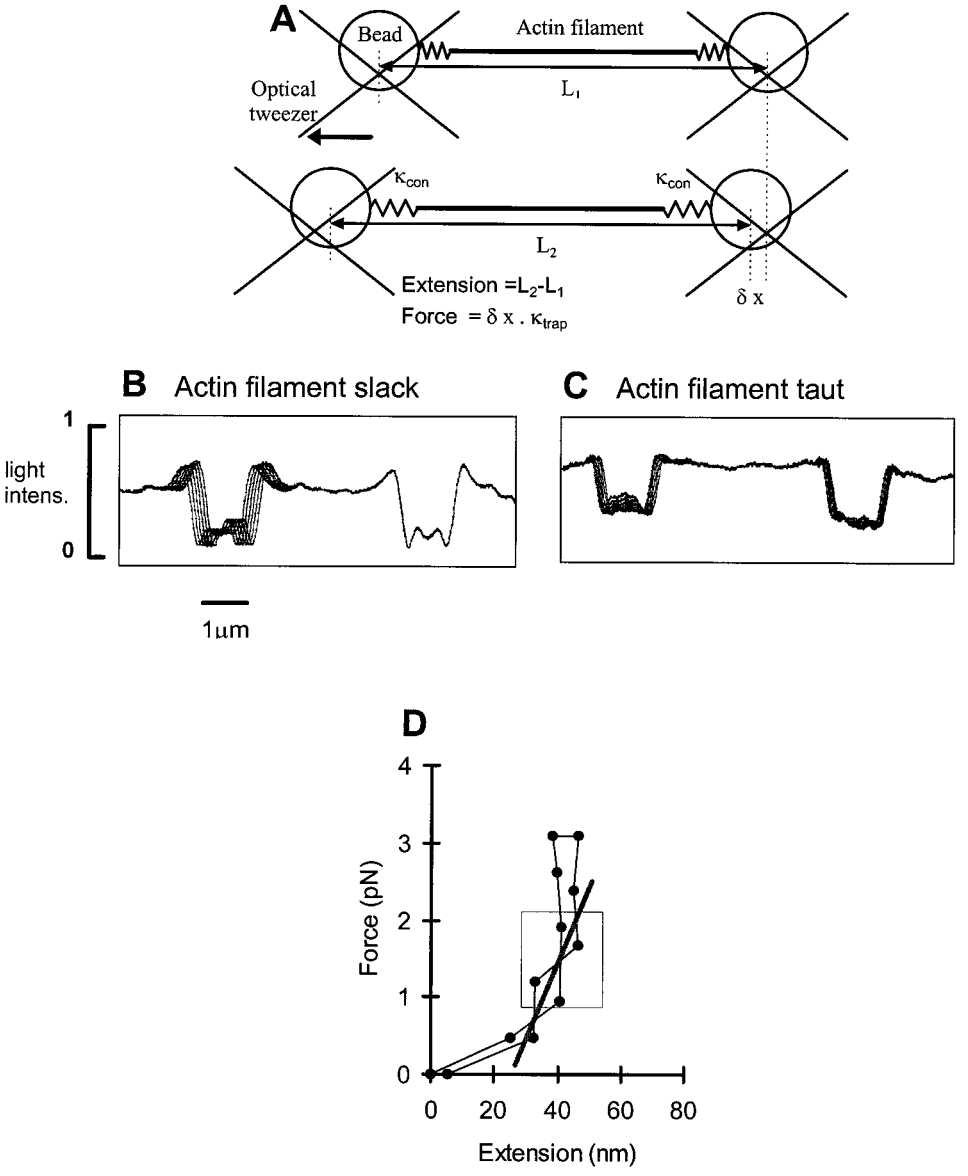

FIGURE 5 (*A*) Static measurements of the bead-actin-bead stiffness using video imaging. Force was applied by stepping the left trap to the left. To determine the position of the beads on the video image, five lines of video data, taken from the central part of the bead image, were averaged over 10 video frames. Bead movements were determined from the position of the center of mass calculated from the video data. Forces were determined from the movement of the right bead. (*B* and *C*) Superposition of six averaged video images. In *B* the actin filament is slack, and when the left bead was displaced the right bead did not move (we found the resolution of this method to be ~2 nm). In *C* the actin filament is held taut between the two beads. Movement of the left trap caused movement of both beads. (*D*) Force-extension diagram of one bead pair for one stretching cycle, which consists of one stretching phase in five steps and a subsequent releasing phase, again in five steps. The least-squares line fitted to the linear part of the curve gives the stiffness κ_{link} in the region of steady tension (1–2 pN) over which other mechanical experiments were performed (in this example 0.13 pN nm^{-1}).

trap stiffnesses (e.g., Fig. 4 *C*, *n* segments r.m.s. deviation = 10–11 nm ≡ 0.33–0.4 pN nm^{-1}; see Eqs. A4 and A5).

κ_{con} and κ_{xb} determined from analysis of Brownian motion

κ_{con} can also be estimated from Brownian motion by extracting the uncorrelated portion of motion of the linked beads (similar in principle to the approach of Mehta et al., 1997). Uncorrelated motion occurs as the beads move either toward or away from each other (rather than motion in the same direction). This releases or extends the series elasticity, κ_{con}. We recorded the motion of both of the beads with the two four-quadrant detectors. The two upper traces in Fig. 6 *B* show the displacement of the left and right beads from a small part of Fig. 6 *A*, but at higher time resolution. The lowest trace shows the difference between the two bead positions, i.e., the uncorrelated motion. The r.m.s. deviation of the uncorrelated motion, when no HMM was attached, is 6 nm. This gives an estimate for κ_{link} of 0.1 pN nm^{-1}, which is similar to the result obtained in the previous section. This method is inaccurate because the small amplitude of the uncorrelated motion suffers from significant contamination from other noise sources. The problem is exacerbated by the parabolic dependence of stiffness upon displacement amplitude. We would require a much more sensitive and lower-noise detector for this method to work well for larger values of κ_{con} (see Fig. 6 *C*).

Knowing κ_{link} and κ_{trap}, κ_{xb} can be derived from the total stiffness measured during cross-bridge attachment (the total stiffness is then given by the series combination of κ_{xb} and κ_{link} in parallel with κ_{trap}; see Appendix, Fig. 11 and Eqs. A6–A8). We found that the Brownian motion during attached intervals was 3–4 nm (r.m.s.; e.g., Fig. 4 *C*, *e*-segments). For the reasons given in the previous paragraph, this gives a poor estimate for κ_{xb} that is in the range of 1–2 pN nm^{-1}.

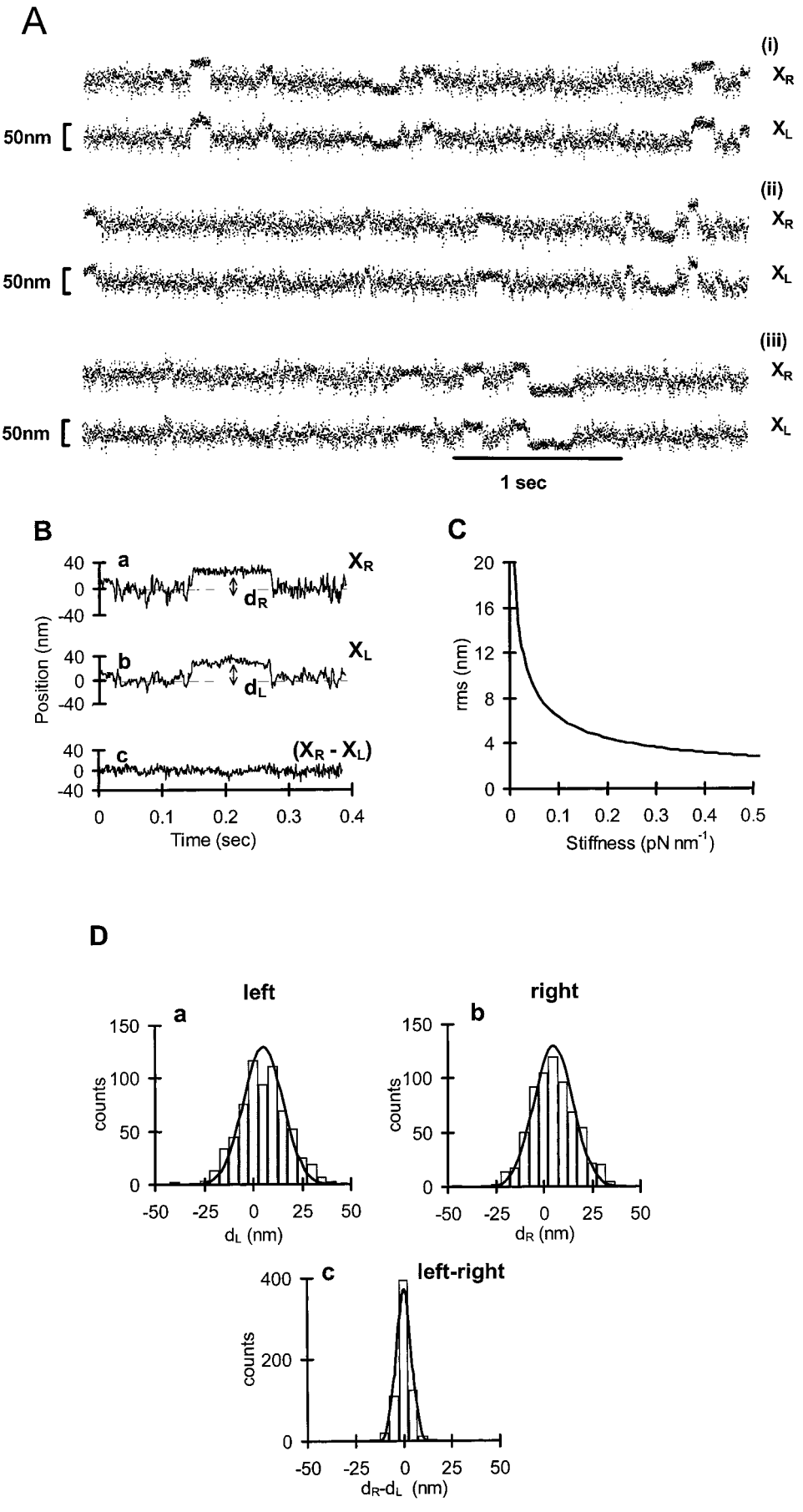

FIGURE 6 (*A*) Simultaneous traces of the displacements of both beads holding an actin filament due to interactions with low densities of HMM (bound to the surface at 1 mg ml^{-1}). Three sequential pairs of records (i–iii) are shown. X_R and X_L show the simultaneous positions of the right and left beads, respectively (ATP concentration 3 μM, 23°C). (*B*) (*a, b*). Part of *A*, but at higher time resolution to show displacements of the bead before, during, and after a single HMM attachment. X_R and X_L show displacements of the right- and left-hand beads holding an actin filament. The mean displacements during the attachments, d_R and d_L, are determined from the mean position during the attachment minus the mean position of the baseline measured before and after the attachment. (*c*) Difference between the traces, $X_R - X_L$. (*C*) Graph of the theoretical value of r.m.s. Brownian motion of a trapped bead, calculated for increasing system stiffnesses (see Appendix). The r.m.s. background noise of the detector was ~1.4 nm (Fig. 4). Analysis of the Brownian noise is of use in determining system stiffness only below values of ~0.1 pN nm^{-1}. (*D*) (*a, b*) Distributions of mean displacements for right-hand and left-hand beads during 666 attachments from four actin-filament preparations. For any bead-actin-bead preparation there is a strong bias in one or another direction (determined by the polarity of the actin filament); this direction was made positive in the histograms. The solid curves are Gaussian distributions. The means are equal to the mean value of the events, the amplitudes were determined from the total counts, and the standard deviations were determined from the thermal motion of the bead position in the absence of attachments. For the left- and the right-beads the mean value was 5.04 nm. (*c*) The difference ($d_R - d_L$) was determined on an event-by-event basis and plotted for the 666 events shown above. The solid curve is the Gaussian curve fitting best to the data, with a midposition at 0.005 ± 3.76 nm (S.D.), e.g., centered close to zero.

In summary, we found that 1) κ_{con} is nonlinear and variable between preparations; 2) at 1–2 pN pretension of the actin filament, $\kappa_{actin} \gg \kappa_{con} \gg \kappa_{trap}$ (but κ_{con} is probably on the same order of magnitude as κ_{xb}); and 3) because of the manner in which the stiffnesses are combined in series and parallel, analysis of Brownian motion gives a poor estimate of κ_{xb} and κ_{con}.

κ_{con} and κ_{xb} determined from forced oscillations

We measured κ_{con} and κ_{xb} separately by driving one optical trap back and forth with a large-amplitude, sinusoidal oscillation while measuring the position of both trapped beads with the two four-quadrant detectors. The position of the bead in the driven trap was used to derive the applied force, and motion of the other bead gave the extension of the cross-bridge and/or the extension of the actin-to-bead connections (Fig. 7).

At an oscillation frequency of 105 Hz and in the absence of cross-bridge attachment, the amplitude of the driven bead motion was approximately half that of the laser motion, and there was a phase shift of ~30°. The phase shift was due to the viscous drag on the beads (Fig. 8 *B, loop b*). The reduced amplitude of bead motion was caused mainly by the stiffness of the other, stationary trap. We made the peak-to-peak motion of the driven (right-hand side) bead (X_R) ~200 nm. In the absence of an attached cross-bridge, the applied forcing function caused both beads to move sinusoidally. The difference in their movement (the gradient of Fig. 8 *C* is greater than 1; see Eq. A9) arises from length changes in the bead-actin-bead assembly as κ_{link} is subjected to the varying load.

During periods of cross-bridge attachment (Fig. 7, labeled a_1-a_3), motion of the driven bead (X_R) was used to calculate the force applied to the cross-bridge, and motion of the passive bead (X_L) measured the cross-bridge exten-

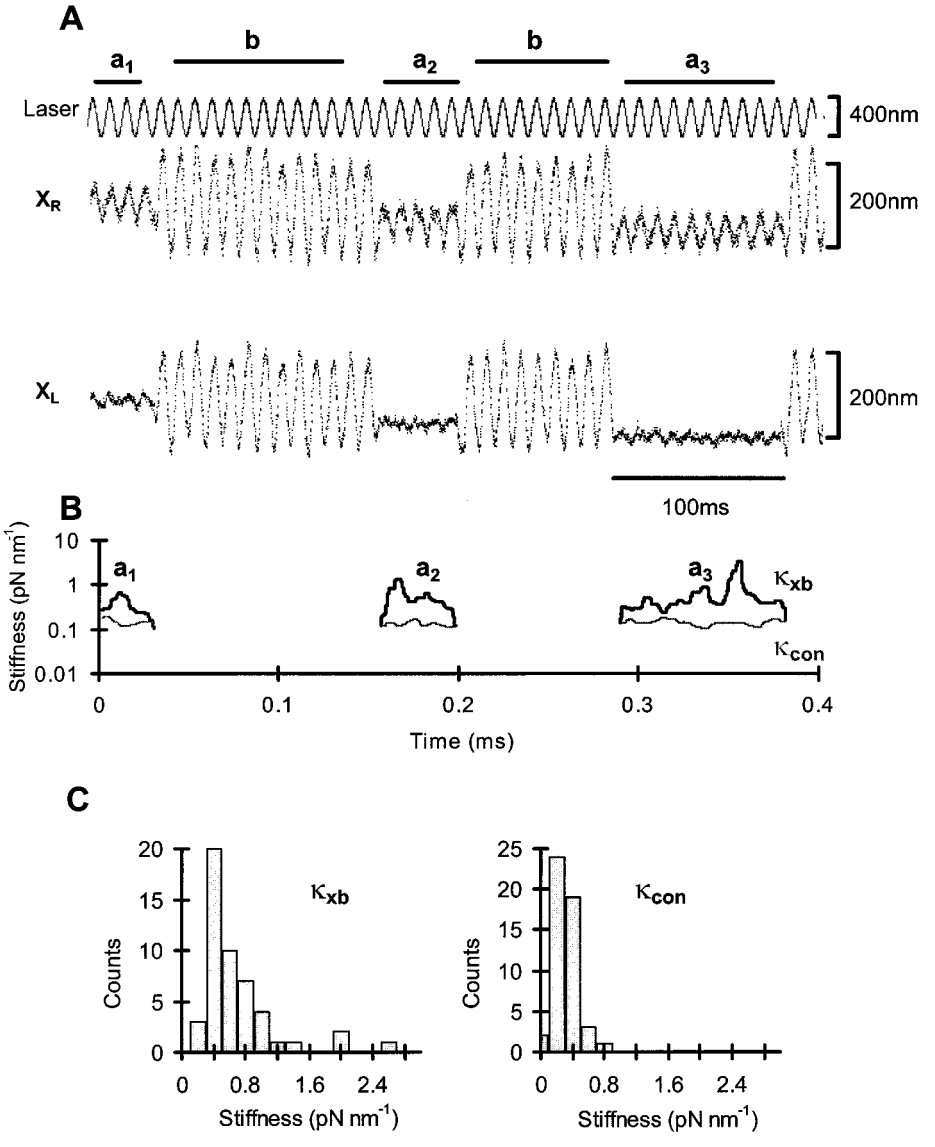

FIGURE 7 Stiffness measurements using two 4QD detectors. (*A*) A 105-Hz sinusoidal waveform was applied to the right laser position while the left laser was held fixed. X_R and X_L show the position of the right and left beads. (*B*) $\kappa_{con,R}$ is given approximately by calculating the quotient of the applied force ($\kappa_{trap} \cdot (x_{trap} - X_R)$) and the length change ($X_R - X_L$). The time course of cross-bridge stiffness κ_{xb} during attachments was calculated from the applied force and the induced myosin length change ($\approx X_L$) with a running discrete Fourier transform. The average stiffness κ_{con} and κ_{xb} during event a_1-a_3 were κ_{xb}: 0.41 ± 0.15 pN nm^{-1}, 0.56 ± 0.29 pN nm^{-1}, 0.60 ± 0.57 pN nm^{-1}; κ_{con}: 0.15 ± 0.03 pN nm^{-1}, 0.13 ± 0.02 pN nm^{-1}, 0.14 ± 0.02 pN nm^{-1}. (*C*) Histogram to show the distribution of the average values of κ_{con} and κ_{xb} measured during 49 attachments, obtained from 20 different myosin molecules (ATP concentration 10 μM, 23°C).

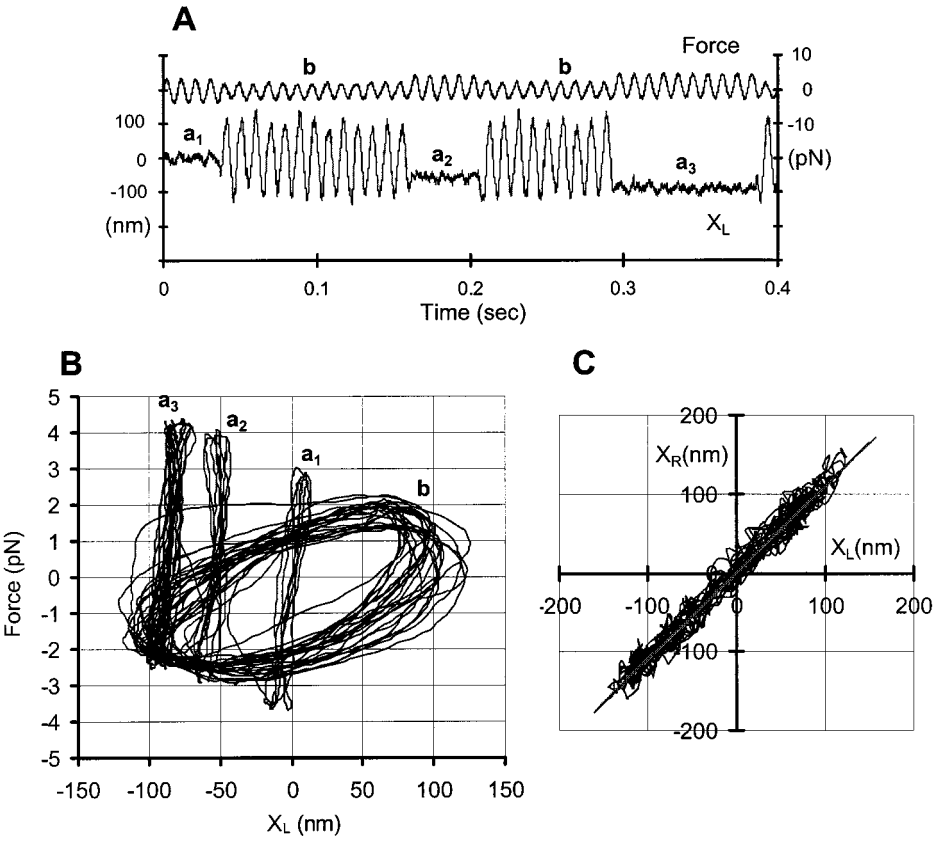

FIGURE 8 (*A*) Applied force (*upper trace*) and movement of the left bead (*lower trace*) from the experimental data shown in Fig. 7 *A*. (*B*) Plotting force against the left bead position gives the stiffness during each attached interval (loops a_1-a_3; 0.38, 0.71, 0.48 pN nm^{-1}, respectively); a correction factor of ~10% should be applied to these slopes to account for κ_{con}. Loop b arises from motion during "detached" intervals. The hysteresis shown by this loop is caused by viscous drag on both beads. (*C*) Left bead versus right bead position during "detached" intervals. There is little phase shift between the motion of the driven (*right*) and the passive (*left*) bead because κ_{link} is large compared to the drag on a single bead (at this forcing frequency); the slope of the curve is given by $\kappa_{link}/(\kappa_{link} + \kappa_{trap})$.

sion. To extract the amplitudes we performed a running discrete Fourier transform at the forcing frequency over a single oscillation period on both the X_R and X_L data. κ_{con} was calculated from the quotient of net extension between the beads and the applied force (Eq. A10). By substituting κ_{con} into Eqs. A12 and A13, κ_{xb} was obtained from Eq. A11. In this way we obtained a running estimate of both κ_{con} and κ_{xb} during each attached interval (Fig. 7 *B*). We could not resolve any systematic change in κ_{xb} or κ_{con} over the attached period. Hence, κ_{xb} and κ_{con} were averaged over each attachment interval and plotted as a histogram (Fig. 7 *C*). The overall mean was 0.69 ± 0.47 pN nm^{-1} for κ_{xb} and 0.31 ± 0.16 pN nm^{-1} for κ_{con}.

κ_{xb} was also determined from a plot of force versus passive bead movement (Fig. 8 *B, loops* a_1, a_2, a_3). In these diagrams the positions of the loops on the *x* axis indicate the starting positions of cross-bridge attachment along the actin filament. The gradient of these diagrams gives κ_{xb}, because the passive bead motion is nearly the same as that of the cross-bridge (average gradient of curves a_1, a_2, a_3 in Fig. 8 $B = 0.52$ pN nm^{-1}).

Displacement produced by a single cross-bridge interaction

By monitoring both bead positions with the two four-quadrant detectors, we were able to address some of the doubts and problems associated with previous estimates of the cross-bridge working stroke, which were made with an apparatus with only a single detector. For example:

1. Does the motion of a single bead correctly measure the motion of the entire bead-actin-bead assembly, i.e., does the system behave as a nearly "rigid dumbbell"?

2. Does the actin filament change length significantly during cross-bridge attachments?

3. Do artifactual displacements arise if the actin filament binds to HMM that is situated with an orthogonal displacement to the filament center line?

1) Inspection of Fig. 6 shows that the motion of the two beads is well correlated. This means that the bead-actin-bead assembly translates as a nearly rigid body under the influence of Brownian motion. Therefore the actin monomers in the vicinity of the HMM (near the center of the filament) must move in a manner similar to that of the beads.

Attachments were detected from the increase in stiffness (Molloy et al., 1995), and the amplitude of each was measured relative to the mean rest positions for the two beads (Fig. 6 *D*). Attachments were detected automatically by calculating the running variance of the position data (five points), applying a median filter (31 points) to the calculated variance, and then thresholding this data. The data associated with attached intervals were removed, and the remaining data were corrected for baseline drift. Attachment event

amplitudes were obtained from the median point in the data relative to corrected baseline at the middle time point of the event. The distributions of event amplitudes, measured separately from data obtained for left and right 4QDs, are shown in Fig. 6 *D*, *a*, *b*. These histograms were fitted well by a single Gaussian distribution, indicating that the data consists of a single population of events. Therefore the mean amplitude of the events was used to measure the average movement produced by the cross-bridge. The spread of the data is explained by the randomizing effect of Brownian motion (Molloy et al., 1995). Both distributions were centered at 5 nm from mean rest position.

2) To determine whether the actin filament changes length during the cross-bridge cycle, the distribution of the difference of left and right bead positions determined on an event-by-event basis was plotted as a histogram (see Fig. 6 *D*, *a–c*). A consistent difference in position would indicate that the actin filament changed length when it interacted with the HMM. The mean value of this difference gives the average extension of the bead-actin-bead assembly during events. We found the difference to be 0.06 ± 3.06 nm (SD). The spread of this distribution is explained by the uncorrelated Brownian motion of the beads, which results from compliance of the bead-actin-bead assembly (κ_{link}; see above).

3) If the actin filament binds to an HMM that is displaced laterally from the filament midline (in the *y* axis), this would produce an artifactual observed displacement. This displacement arises because the midpoint of the actin filament would be pulled laterally, and the two beads would therefore move closer together. For example, if the center of a 5-μm-long actin filament bound to an HMM that was 100 nm from the average midline position of the filament, each bead would move ~2 nm inward. If the myosin then underwent a working stroke, the effect would be to increase the observed displacement of one bead and reduce that of the other. However, we found that the average displacement for left and right beads was 5.042 nm and 5.037 nm (respectively), so this potential source of artifact did not seem to affect our results.

DISCUSSION

The aim of this study was to obtain an estimate of the stiffness and working stroke produced by a single acto-HMM interaction under in vitro conditions. The objective was to test if the working stroke and stiffness are consistent with current ideas of how actomyosin functions to produce force and movement. In summary, we found that it was necessary to measure series elastic components in the system and that extension of these components during cross-bridge interactions produced a small measurement error in the working stroke, but a large error in cross-bridge stiffness. Furthermore, by measuring the position of both beads, we found that actin filament length remained constant during cross-bridge interactions, and the segment of the actin filament that is able to interact with the HMM molecule moved by approximately the same amount as the beads held in the optical traps.

Series elasticity and cross-bridge stiffness

Dupuis et al. (1997) discovered that the bead-actin-bead assembly used in these studies has considerable "end compliance" (or connection stiffness κ_{con}). Their explanation was that extensibility arose from a combination of actin filament flexure at the point of attachment of actin to the trapped bead and rotation of the bead within the optical trap. We measured the long-range series elasticity of our bead-actin-bead assemblies by video microscopy. At the trap stiffness used in our experiments, the maximum pretension that could reasonably be applied (~2 pN) was insufficient to extend this nonlinear series compliance to a suitably high stiffness; i.e., κ_{con} (0.2 pN nm^{-1}) was lower than the expected value of cross-bridge stiffness (2 pN nm^{-1}; Huxley and Tideswell, 1997). Analysis of the mechanical system (see Appendix, Fig. 9, and Fig. 6 *C*) indicated that estimates obtained by measurement of Brownian motion would give inaccurate estimates of cross-bridge stiffness. Therefore, we developed a novel technique for measuring the cross-bridge stiffness more directly. A force was applied to the cross-bridge by driving one optical trap back and forth with a sinusoidal motion. Cross-bridge distortion was measured from the motion of the other bead held in the fixed optical trap. Using this technique, we found cross-bridge stiffness to be ~0.7 pN nm^{-1}. Recently, Mehta et al. (1997) obtained a similar value of 0.65 pN nm^{-1} for the stiffness of a single rabbit HMM cross-bridge. They used a trapping geometry identical to that employed here and determined cross-bridge stiffness by a method based on analysis of Brownian motion. Nishizaka et al. (1995) measured HMM cross-bridge stiffness by using a single bead held in an optical tweezer that was attached to the end of an actin filament by gelsolin. Use of gelsolin should reduce actin filament flexure, because it binds to the end of the filament. However, they still found a nonlinear length-tension diagram at low force that extended over 30 nm. Their estimate of cross-bridge stiffness, 0.58 pN nm^{-1}, obtained from the steepest region of the curve, is similar to the value we report here.

Several recent studies (e.g., Irving et al., 1995) indicate that the regulatory domain of the myosin head tilts during the working stroke and is distorted by load (Lombardi et al., 1995). If the elasticity resides within the head of the myosin molecule, it is important to ask whether a "cross-bridge" consists of one or both heads of myosin. In this study, we used two-headed HMM, so potentially both heads might bind to actin. If the regulatory domain of each head contributes equally to stiffness, then we might expect the stiffness to be double that of a single head. However, it may be that only one of the two HMM heads can form a stiff connection to actin, as has been suggested for muscle fibers (Offer and Elliott, 1978; Huxley and Tideswell, 1997).

Series elasticity and the working stroke

We have shown that because $\kappa_{con} \gg \kappa_{trap}$, the bead-actin-bead assembly used in these experiments oscillates back and forth as a nearly rigid body, under the influence of Brownian motion. On average, the HMM molecule could interact with any actin monomer that comes within range. This means that the starting point of any individual displacement is unknown and simply cannot be measured for a single observation. Instead, a large number of displacements must be measured and averaged. The expected distribution of displacement amplitudes will have the same r.m.s. deviation as the Brownian noise of the bead-actin-bead assembly. Consequently, if we know the standard deviation of the expected distribution from the overall system stiffness, κ_x, we can calculate the accuracy of our estimate of the displacement from the standard error of the mean. We measured 666 attachments, which had an average observed displacement of 5.0 nm and a standard error of the mean of $\pm$0.4 nm ((r.m.s. of Brownian noise)/$(n)^{0.5}$). Because κ_{con} is in series with κ_{trap}, it will be extended by the cross-bridge working stroke, and so the observed bead displacement is smaller than the working stroke. From our measurements of κ_{con} and κ_{trap}, the working stroke will be 10% larger than the displacement measured directly from the bead motion. The working stroke is therefore 5.5 $\pm$ 0.4 nm (SEM).

We found no change in length of the actin filament caused by its interaction with HMM. During each interaction the entire bead-actin-bead assembly is translated by ~5 nm by the cross-bridge. Therefore, we have shown that length changes in the actin filament neither cause nor contribute significantly to the movement produced by actomyosin interactions at low load.

Cross-bridge working-stroke, stiffness, and energy transduction

The best estimates of mechanical work done per ATP hydrolyzed in muscle fibers come from experiments that were performed to determine the efficiency of muscle contraction. Frog sartorius muscle is the best studied muscle type. Kushmerick and Davies (1969) found that frog sartorius produced 38 pN nm per ATP hydrolyzed (average of their three highest estimates, multiplied by 115% to account for extra ATP usage by Ca^{2+} pumping, as suggested by Woledge et al., 1985). Huxley and Simmons (1971) suggested a similar value of 30 pN nm (7.3kT) per interaction. The best recent estimate, based purely on fiber mechanical properties (Linari et al., 1998), produces a value of 27 pN nm per working stroke.

To summarize our results: We have found that κ_{xb} is 0.7 pN nm^{-1}, and the cross-bridge working stroke, d_{xb}, is 5.5 nm. Using these values, it is straightforward to calculate the mechanical work done per interaction, e.g., $\frac{1}{2}d_{xb}^2 \times \kappa_{xb}$ = 11 pN nm. This is only one-third of the value obtained from frog muscle fibers. There are several possible explanations and we list their pros and cons below:

1. The mechanical work performed by each actomyosin interaction might be lower in rabbit back muscle than in frog sartorius muscle. We know of no good estimates of work done per ATP hydrolyzed by rabbit fast muscle. There is known to be variability between muscle type and species; higher values have been reported for tortoise muscle (Woledge, 1968) and much lower values for insect flight muscle (Ellington, 1985).

2. The force produced by myosin may be constant over the working stroke. This would make our estimate twice as large as those given above, e.g., work = $d_{xb}^2 \times \kappa_{xb}$. The data of Fig. 8 *B* (curves a_1, a_2, and a_3) are too noisy to determine whether cross-bridge stiffness is strictly linear, so we cannot rule out the possibility that myosin exerts a nearly constant force during its working stroke. Highly nonlinear elasticity is not easily compatible with most mechanistic schemes for cross-bridge behavior (e.g., Pate and Cooke, 1989).

3. One or both of our measurements (e.g., d_{xb} or κ_{xb}) may underestimate values obtained in the well-ordered filament lattice of muscle fibers.

d_{xb}: Previously (Molloy et al., 1995) we noted that myosin head orientation may affect the size of the observed movement produced by the cross-bridge. HMM molecules that are randomly oriented with respect to the actin filament might produce a mean estimate of the working stroke that is determined by averaging a cosine term through 180°. This would lead to an underestimation of the "true" working stroke produced by correctly oriented HMM molecules by a factor of $\pi/2$. The highly ordered thick and thin filament arrays found in muscle sarcomeres ensure that all of the myosin molecules are aligned parallel to the axis of the actin filament. Ishijima et al. (1996) measured d_{xb} using synthetic myosin rod cofilaments and report a much longer working stroke (17 nm). This value is so large that it is not easily compatible with the idea of a change in cross-bridge conformation causing the movement.

κ_{xb}: Our in vitro measurement of cross-bridge stiffness might not reflect the stiffness of a cross-bridge in a muscle fiber. HMM bound to a nitrocellulose surface may be either stiffer or more compliant than that of a myosin embedded in a thick filament in muscle. If we take our highest estimates of κ_{xb} (2 pN nm^{-1}), then the mechanical work done per working stroke would be 30 pN nm. It is interesting to note that κ_{xb} measured using synthetic myosin rod cofilaments, with correctly oriented myosin heads (Ishijima et al., 1996; 0.14 pN nm^{-1}), was smaller than ours obtained with HMM fixed to nitrocellulose. Such low values of stiffness require either long or multiple working strokes per ATP.

4. There may be more than one cross-bridge interaction per ATP hydrolyzed, and hence the mechanical work done per ATP might be higher. This idea has been proposed for the cross-bridge cycle occurring in muscle fibers that are allowed to shorten rapidly under low load (Piazzesi and Lombardi, 1995). However, we find that the lifetime of the attachments observed here under low load show a first-order dependence upon ATP concentration (data not shown). So it

is most likely that each of the mechanical interactions observed is terminated by the binding of one ATP molecule.

The calculated basic free energy change for ATP breakdown under the in vitro conditions used here is ~ -60 kJ mol^{-1} ($\equiv$ 100 pN nm). This is almost twice the energy available in a muscle fiber under physiological conditions (-35 kJ mol^{-1} for creatine phosphate; Woledge and Reilly, 1988). We think it is incorrect to multiply the in vitro basic free energy by an efficiency factor obtained under physiological chemical conditions to obtain a value for expected work output for a single molecule in vitro. To do so would imply that the working stroke or cross-bridge stiffness depends upon ligand concentration. So far we find no evidence for this.

The amount of mechanical work done per ATP hydrolyzed by different myosins under different mechanical and chemical conditions remains an open question. Our measurement of the maximum work obtainable per ATP hydrolyzed under these in vitro conditions is only one-third of that measured in intact frog muscle fibers. However, our results are not inconsistent with current ideas of how actomyosin works.

APPENDIX

Force transducer consisting of a single trapped bead

The properties of this kind of transducer have been described in detail elsewhere (e.g., Svoboda and Block, 1994). Examination of this system reveals the basic properties of the optical tweezers transducer. The equation of motion of the trapped bead in solution is

$$m\frac{\partial^2 x}{\partial t^2} + \beta\frac{\partial x}{\partial t} + \kappa x = 0 \tag{A1}$$

where m is the bead mass, x is the displacement of the bead from the trap center, β is the viscous drag, and κ_{trap} is the trap stiffness (Fig. 9). For most optical trap experiments, κ_{trap} is adjusted to be $\sim$0.02 pN nm^{-1}. For a 1-μm-diameter bead suspended in water, inertial forces are negligible compared to the viscous damping and elastic trapping force, so the first term of Eq. A1 can be ignored. Thermally driven bead motion (Brownian motion) is characterized by a Lorentzian power spectrum with a cutoff frequency (f_c) determined by the ratio of trap stiffness to viscous drag coefficient:

$$f_c = \kappa_{trap}/(2\pi\beta) \tag{A2}$$

(e.g., for a 1-μm bead suspended in water; $\beta = 6\pi\eta\alpha \cong 10^{-5}$ pN s nm^{-1}; $f_c \cong 330$ Hz).

If the viscous drag coefficient is known, the measured cutoff frequency can be used to calibrate trap stiffness. However, β depends critically on the proximity of the bead to the glass surface, doubling when a 1-μm-diameter bead is moved from 2 μm above to 1 μm above the surface (Svoboda and Block, 1994). Hence calibration of trap stiffness by this method is unreliable during actomyosin interactions because the viscous drag coefficient is hard to measure.

A second method for determining trap stiffness is to measure the mean squared deviation in bead position ($\langle x^2\rangle$). Trap stiffness can be calculated by applying the equipartition theorem:

$$\kappa_{trap} = \frac{kT}{\langle x\rangle^2} \tag{A3}$$

(e.g., if $\kappa_{trap} = 0.02$ pN nm^{-1}, kT (thermal energy) ≈ 4 pN nm; $\langle x\rangle^2 = 200$ nm^2, hence the r.m.s. deviation = 14 nm).

Stiffness calculations from this relationship are independent of viscous drag and can be used to measure compliant, spring-like elements. However, the sensitivity of this method is lower at high stiffness because of the quadratic dependence of stiffness upon x position (Fig. 6 *C*). Calibration of the position detector and measurement and correction for system noise are crucial when high stiffnesses are measured.

Transducers based on a two-bead system

For two beads connected by a rigid filament, the total axial stiffness (κ_x) measured parallel to the filament will be the sum of the two trap stiffnesses. The two trap stiffnesses combine in parallel, not in series, as might first appear from Fig. 10.

If the linkage is compliant (κ_{link}, Fig. 10), the axial stiffness, κ_x (when both trap stiffnesses are the same), is given by

$$\kappa_x = \frac{\kappa_{trap} \times \kappa_{link}}{\kappa_{trap} + \kappa_{link}} + \kappa_{trap} \tag{A4}$$

where

$$\frac{1}{\kappa_{link}} = \frac{1}{\kappa_{con,R}} + \frac{1}{\kappa_{actin}} + \frac{1}{\kappa_{con,L}}$$

(see Fig. 11).

If $\langle x^2\rangle$ and κ_{trap} are known, κ_{link} can be calculated from Eqs. A3 and A4:

$$\langle x^2\rangle = kT\left(\frac{1}{\kappa_x}\right) = \frac{kT}{2}\left(\frac{1}{\kappa_{trap}} + \frac{1}{(\kappa_{trap} + 2\times\kappa_{link})}\right) \tag{A5}$$

(e.g., κ_x varies between κ_{trap} and $2\kappa_{trap}$ for values of κ_{link} between 0 and ∞, and analysis of Brownian motion gives a good estimate of κ_{link} only if κ_{link} is similar to κ_{trap}).

During attachment, cross-bridge stiffness, κ_{xb}, changes the mechanical properties of the system:

$$\kappa_A = \frac{\kappa_{trap} \times \kappa_{con,L}}{\kappa_{trap} + \kappa_{con,L}} \approx \kappa_{trap} \qquad \text{for } \kappa_{con} \gg \kappa_{trap} \tag{A6}$$

$$\kappa_B = \kappa_A + \kappa_{xb} \approx \kappa_{xb} \qquad \text{for } \kappa_{xb} \gg \kappa_A \tag{A7}$$

$$\kappa_X = \frac{\kappa_{con,R} \times \kappa_B}{\kappa_{con,R} + \kappa_B} + \kappa_{trap} \approx \frac{\kappa_{con,R} \times \kappa_{xb}}{\kappa_{con,R} + \kappa_{xb}} \tag{A8}$$

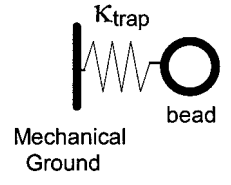

FIGURE 9 Force transducer consisting of a single trapped bead.

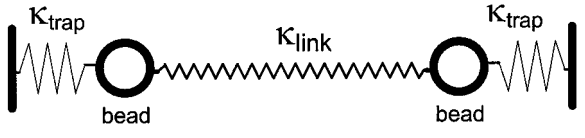

FIGURE 10 Transducers based on a two-bead system.

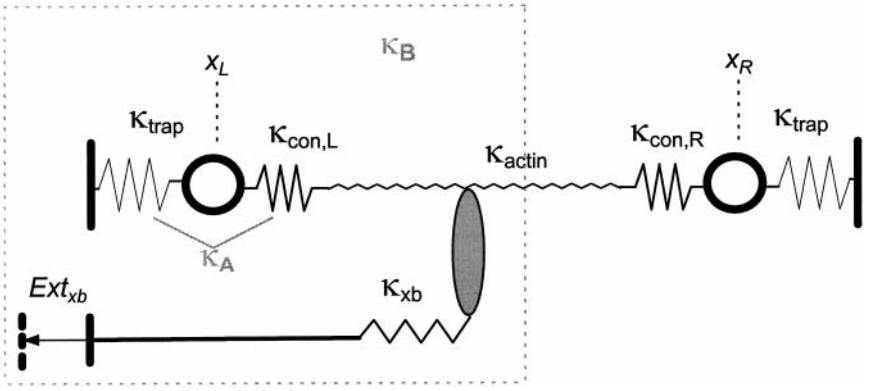

FIGURE 11 Components of κ_{link}.

where κ_{xb} and $\kappa_{con} \gg \kappa_{trap}$; κ_x is composite stiffness parallel to the actin filament (x direction); $X_{L,R}$ is the position of the left, right bead; κ_{trap} is trap stiffness; κ_{actin} is actin filament stiffness; $\kappa_{con\ L,R}$ is the actin-to-bead connection left, right; κ_{xb} is the cross-bridge stiffness; and Ext_{xb} is the cross-bridge extension.

During cross-bridge attachment, κ_x is dominated by κ_{con} and κ_{xb} in series. κ_{xb} can be found by analyzing Brownian motion if $\kappa_{con} \gg \kappa_{xb}$. Otherwise κ_{con} and κ_{xb} must be determined independently. To do this we applied a sinusoidal forcing function to the position of one trap (x_{trap}) and observed the positions of both beads (x_L and x_R). The analysis below assumes that 1) the right trap is moved and the left trap is fixed (e.g., x_{trap} is the position of the right trap); 2) κ_{actin} is much greater than other stiffnesses in the system; 3) $\kappa_{xb} \gg \kappa_{trap}$; 4) $\kappa_{con} = \kappa_{con,R} = \kappa_{con,L}$.

During periods when no cross-bridge is attached, κ_{con} is given by

$$\kappa_{con} = 2 \times \kappa_{trap} \times \frac{x_{trap} - x_R}{x_R - x_L} \tag{A9}$$

During periods of cross-bridge attachment, κ_{con} is given by

$$\kappa_{con} = \kappa_{trap} \times \frac{x_{trap} - x_R}{x_R - x_L} \tag{A10}$$

where $(x_{trap} - x_R)$ and $(x_R - x_L)$ are the in-phase amplitudes determined by discrete Fourier transform of the data (either as a running window of one cycle or averaged over the entire observation interval). κ_{xb} is given by the quotient of force applied to the cross-bridge and its extension:

$$\kappa_{xb} = \frac{F_{xb}}{Ext_{xb}} \tag{A11}$$

where

$$Ext_{xb} = X_L \times \frac{\kappa_{con} + \kappa_{trap}}{\kappa_{con}} \tag{A12}$$

$$F_{xb} = \kappa_{trap} \times (x_{trap} - x_R) - \kappa_A \times Ext_{xb} \tag{A13}$$

Note that if $\kappa_{con} \gg \kappa_{trap}$, then left bead movement $x_L \approx Ext_{xb}$

Finally, estimates of the cross-bridge working stroke from the mean of the histogram of observed bead displacements ($d_{observed}$) should be corrected for extension of the series elastic elements:

$$\text{xb work stroke} = \frac{\kappa_{con} + \kappa_{trap} + (2 \times \kappa_{con} \times \kappa_{trap})/\kappa_{xb}}{\kappa_{con}} \times d_{observed} \tag{A14}$$

We thank Prof. A. F. Huxley for helpful comments on an earlier version of the manuscript and Dr. A. E. Knight, Dr. R. Thieleczek, and Dr. R. T. Tregear for many helpful discussions.

This work was funded by the Biotechnology and Biological Sciences Research Council, the Royal Society (of London), and the British Heart Foundation.

REFERENCES

Cooke, R. 1998. Actomyosin interaction in striated muscle. *Physiol. Rev.* 77:671–697.

Dupuis, D. E., W. H. Guilford, J. Wu, and D. M. Warshaw. 1997. Actin filament mechanics in the laser trap. *J. Muscle Res. Cell Motil.* 18: 17–30.

Ellington, C. P. 1985. Power and efficiency of insect flight muscle. *J. Exp. Biol.* 115:293–304.

Finer, J. T., R. M. Simmons, and J. A. Spudich. 1994. Single myosin molecule mechanics: piconewton forces and nanometre steps. *Nature.* 386:113–119.

Guilford, W. H., D. H. Dupuis, G. Kennedy, J. Wu, J. B. Patlak, and D. M. Warshaw. 1997. Smooth and skeletal muscle myosin produce similar forces and displacements in the laser trap. *Biophys. J.* 72:1006–1021.

Huxley, A. F., and R. M. Simmons. 1971. Proposed mechanism of force generation in striated muscle. *Nature.* 233:533–538.

Huxley, A. F., and S. Tideswell. 1997. Filament compliance and tension transients in muscle. *J. Muscle Res. Cell Motil.* 17:507–511.

Huxley, H. E. 1969. The mechanism of muscular contraction. *Science.* 164:1356–1366.

Irving, M., T. S. Allen, C. Sabidodavid, J. S. Craik, B. Brandmeier, J. Kendrick-Jones, J. E. T. Corrie, D. R. Trentham, and Y. E. Goldman. 1995. Tilting of the light-chain region of myosin during step length changes and active force generation in skeletal muscle. *Nature.* 375: 688–691.

Ishijima, A., H. Kojima, H. Higuchi, Y. Harada, T. Funatsu, and T. Yanagida. 1996. Multiple and single molecule analysis of the actomyosin motor by nanometer piconewton manipulation with a microneedle: unitary steps and force. *Biophys. J.* 70:383–400.

Kojima, H., A. Ishijima, and T. Yanagida. 1994. Direct measurements of stiffness of single actin filaments with and without tropomyosin by in vitro nanomanipulation. *Proc. Natl. Acad. Sci. USA.* 91:12962–12966.

Kron, S. J., Y. Y. Toyoshima, T. Q. P. Uyeda, and J. A. Spudich. 1991. Assays for actin sliding movement over myosin-coated surfaces. *Methods Enzymol.* 196:399–416.

Kushmerick, M. J., and R. E. Davies. 1969. The chemical energetics of muscle contraction. II. The chemistry, efficiency and power of maximally working sartorius muscles. *Proc. R. Soc. Lond. Biol.* 174:315–353.

Linari, M., I. Dobbie, M. Reconditi, N. Koubassova, M. Irving, G. Piazzesi, and V. Lombardi. 1998. The stiffness of skeletal muscle in isometric contraction and rigor: the fraction of myosin heads bound to actin. *Biophys. J.* 74:2459–2473.

Lombardi, V., G. Piazzesi, M. A. Ferenczi, H. Thirlwell, I. Dobie, and M. Irving. 1995. Elastic distortion of myosin heads and repriming of the working stroke in muscle. *Nature.* 374:553–555.

Lymn, R. W., and E. W. Taylor. 1971. Mechanism of adenosine triphosphate hydrolysis by actomyosin. *Biochemistry.* 21:1925–1928.

Margossian, S. S., and S. Lowey. 1982. Preparation of myosin and its subfragments from rabbit skeletal muscle. *Methods Enzymol.* 85:55–71.

Meeusen, R., and Z. Cande. 1979. *N*-Ethylmaleimide-modified heavy meromyosin, a probe for actomyosin interactions. *J. Cell Biol.* 82: 57–65.

Mehta, A. D., J. T. Finer, and J. A. Spudich. 1997. Detection of single molecule interactions using correlated thermal diffusion. *Proc. Natl. Acad. Sci. USA.* 94:7927–7931.

Molloy, J. E. 1997. Optical chopsticks: digital synthesis of multiple optical traps. *Methods Cell Biol.* 55:205–216.

Molloy, J. E., J. E. Burns, J. Kendrick-Jones, R. T. Tregear, and D. C. S. White. 1995. Movement and force produced by single myosin head. *Nature.* 378:209–212.

Nishizaka, T., H. Miyata, H. Yoshikawa, S. Ishiwata, and K. Kinosita, Jr. 1995. Unbinding force of a single motor molecule of muscle measured using optical tweezers. *Nature.* 377:251–254.

Offer, G., and A. Elliott. 1978. Can a myosin molecule bind to two actin filaments? *Nature.* 271:325–329.

Pardee, J. D., and J. A. Spudich. 1982. Purification of muscle actin. *Methods Cell Biol.* 24:274–289.

Pate, E., and R. Cooke. 1989. A model of cross-bridge action: the effects of ATP, ADP and P_i. *J. Muscle Res. Cell Motil.* 10:181–196.

Piazzesi, G., and V. Lombardi. 1995. A cross-bridge model that is able to explain mechanical and energetic properties of shortening muscle. *Biophys. J.* 68:1966–1979.

Rayment, I., H. M. Holden, M. Whittaker, C. B. Yohn, M. Lorenz, K. C. Holmes, and R. A. Milligan. 1993. Structure of the actin-myosin complex and its implications for muscle contraction. *Science.* 261:58–65.

Saito, K., T. Aoki, and T. Yanagida. 1994. Movement of single myosin filaments and myosin step size on an actin filament suspended in solution by a laser trap. *Biophys. J.* 66:769–777.

Simmons, R. M., J. T. Finer, S. Chu, and J. A. Spudich. 1996. Quantitative measurements of forces and displacement using an optical trap. *Biophys. J.* 70:1813–1822.

Svoboda, K., and S. M. Block. 1994. Biological applications of optical forces. *Annu. Rev. Biophys. Biomol. Struct.* 23:247–85.

Veigel, C., D. C. S. White, and J. E. Molloy. 1997. Single molecule energy transduction. *Biophys. J.* 72:A56.

Woledge, R. C. 1968. The energetics of tortoise muscle. *J. Physiol. (Lond.).* 197:685–707.

Woledge, R. C., N. A. Curtin, and E. Homsher. 1985. Energetic aspects of muscle contraction. *Monogr. Physiol. Soc.* 41:167–275.

Woledge, R. C., and P. C. Reilly. 1988. Molar enthalpy change for hydrolysis of phosphorylcreatine under conditions in muscle cells. *Biophys. J.* 54:97–104.